Direct Observation of a Consecutive Two-Step Electron Transfer in Some Zinc Porphyrin–Pyromellitimide–Quinone Triads Which Undergo the Same Mode of Electron Transfers as in the Bacterial Photosynthetic Reaction Center

Masaya Ohkohchi,[1a] Akiko Takahashi,[1a] Noboru Mataga,*,†,[1a] Tadashi Okada,[1a] Atsuhiro Osuka,*,[1b] Hiroko Yamada,[1b] and Kazuhiro Maruyama[1b]

Contribution from the Department of Chemistry, Faculty of Engineering Science, Osaka University, Toyanaka, Osaka 560, Japan, and Department of Chemistry, Faculty of Science, Kyoto University, Kyoto 606, Japan

Received February 2, 1993®

Abstract: Intramolecular photoinduced electron transfer in a series of triads composed of zinc porphyrin (ZnP), pyromellitimide (Im), and quinone (Q) has been investigated by means of picosecond transient absorption spectroscopy to observe directly a two-step electron transfer, the reaction mode of which is the same as that occurring in the biological photosynthetic reaction center. Intramolecular charge separation in ^{1}(ZnP)*–Im–Q gives an initial ion pair (IP) state [(ZnP)$^+$–(Im)$^-$–Q], in which the charge shift reaction leading to formation of a secondary IP state [(ZnP)$^+$–Im–(Q)$^-$] occurs in competition with charge recombination deactivation to the ground state. This two-step electron transfer has been observed directly by monitoring the rise and decay kinetics of a characteristic sharp absorption band due to (Im)$^-$: ^{1}(ZnP)*–Im–Q → (ZnP)$^+$–(Im)$^-$–Q → (ZnP)$^+$–Im–(Q)$^-$. Rates of the charge shift reaction can be controlled by changing the reduction potential of Q, and an approximately 100% quantum yield for the formation of (ZnP)$^+$–Im–(Q)$^-$ from ^{1}(ZnP)*–Im–Q has indeed been realized in a triad bearing trichloro-1,4-benzoquinone as the second electron acceptor owing to an overwhelmingly faster charge shift reaction than charge recombination in the (ZnP)$^+$–(Im)$^-$–Q state.

1. Introduction

In relation to the photoinduced charge separation (CS) mechanism in the natural photosynthetic reaction center (RC), many model compounds have been prepared in an effort to understand factors which control electron transfer (ET) reactions in these highly complex systems.[2-6] Elucidation of three-dimensional structures of bacterial RC[7] has exerted a great impact on such investigations. Recently, increased attention has been paid to conformationally restricted, structurally and energetically well-defined models, some of which mimic some aspects of photosynthetic energy and electron transfer.[4-6] Nevertheless, achievement of nearly quantitative CS by a series of short-range, fast, and efficient ET steps in artificial systems remains very difficult. A basic goal of biomimetic photoinduced ET is to generate with high quantum yield a charge-separated state that stores a maximal amount of the excitation energy as chemical potential energy and that is sufficiently long-lived that this chemical potential can be utilized by subsequent chemical reactions. This may be achieved by introducing a series of electron relay molecules between the initial donor and the ultimate acceptor. The forward ET reactions consist of a series of exergonic steps, each of which can occur quickly and with high quantum yield. The charge recombination (CR) to the ground state, however, will be slow because of the large spatial separation between the primary donor and the ultimate acceptor. Photosynthetic reaction centers use this concept of multistep ET reactions to achieve a high quantum yield for CS across the photosynthetic membrane.

Among the many models studied, much attention has been focused on quinone-linked porphyrins (P–Q). In some strongly polar solutions, CR in a photochemically produced ion pair (IP) state (P)$^+$–(Q)$^-$ has been shown, by means of the direct measurements with ultrafast laser photolysis methods, to proceed much faster than CS in ^{1}(P)*–Q, either in the case of the system linked by short methylene chains or unlinked systems.[8-10] Similar results have been observed also in the case of the porphyrin–pyromellitimide systems (P–Im)[11] as well as the P–Q systems[12,13] linked with more ridig spacers. This can be accounted for by considering energy gap dependencies of photoinduced CS and CR of the IP state for a variety of P–Q systems.[12-14] The energy gap, $-\Delta G_{IP}$ (the energy gap between the IP and ground state) for the CR in strongly as well as moderately polar solutions is around 1.0–1.5 eV, where the CR rate, k_{CR}, is very large, being near the

† Present affiliation: Institute for Laser Technology, Utsubo-Hommachi 1-8-4, Nishiku, Osaka 550, Japan.

® Abstract published in *Advance ACS Abstracts*, November 1, 1993.

(1) (a) Osaka University. (b) Kyoto University.

(2) Boxer, S. G. *Biochim. Biophys. Acta* **1983**, *726*, 265.

(3) Connolly, J.; Bolton, J. R. In *Photoinduced* Electron Transfer; Fox, M. A., Chanon, M., Eds.; Elsevier: Amsterdam, 1988; Part D, p 303.

(4) (a) Wasielewski, M. R. *Photochem. Photobiol.* **1988**, *47*, 923. (b) Wasielewski, M. R. In *Photoinduced Electron Transfer*; Fox, M. A., Chanon, M., Eds.; Elsevier: Amsterdam, 1988; Part A, p 161. (c) Wasielewski, M. R. *Chem. Rev.* **1992**, *92*, 435.

(5) Gust, D.; Moore, T. A. *Science* **1989**, *244*, 35.

(6) Maruyama, K.; Osuka, A. *Pure Appl. Chem.* **1990**, *62*, 1511.

(7) (a) Deisenhofer, J.; Epp, O.; Miki, K.; Huber, R.; Michel, H. *J. Biol. Chem.* **1984**, *180*, 385. (b) Chang, C.-H.; Tiede, D. M.; Tang, J.; Norris, J. R.; Schiffer, M. *FEBS Lett.* **1986**, *205*, 82. (c) Allen, J. P.; Feher, G.; Yeates, T. O.; Komiya, H.; Rees, D. C. *Proc. Natl. Acad. Sci. U.S.A.* **1987**, *84*, 5730.

(8) (a) Mataga, N.; Karen, A.; Okada, T.; Nishitani, S.; Kurata, N.; Sakata, Y.; Misumi, S. *J. Am. Chem. Soc.* **1984**, *106*, 2442. (b) Mataga, N.; Karen, A.; Okada, T.; Nishitani, S.; Sakata, Y.; Misumi, S. *J. Phys. Chem.* **1984**, *88*, 4650.

(9) Mataga, N.; Karen, A.; Okada, T.; Nishitani, S.; Kurata, N.; Sakata, Y.; Misumi, S. *J. Phys. Chem.* **1984**, *88*, 5138.

(10) (a) Wasielewski, M. R.; Niemczyk, M. P.; Svec, W. A.; Pewitt, E. B. *J. Am. Chem. Soc.* **1985**, *107*, 1080. (b) Gaines, G. L., III; O'Neil, M. P.; Svec, W. A.; Niemczyk, M. P.; Wasielweski, M. R. *J. Am. Chem. Soc.* **1991**, *113*, 719.

(11) Osuka, A.; Nakajima, S.; Maruyama, K.; Mataga, N.; Asahi, T. *Chem. Lett.* **1991**, 1003.

(12) Heitele, H.; Pöllinger, F.; Kremer, K.; Michel-Beyerle, M. E.; Futscher, M.; Voit, G.; Weiser, J.; Staab, H. A. *Chem. Phys. Lett.* **1992**, *188*, 270.

(13) Asahi, T.; Ohkohchi, M.; Matsuzaka, R.; Mataga, N.; Zhang, R. P.; Osuka, A.; Maruyama, K. *J. Am. Chem. Soc.* **1993**, *115*, 5665.

(14) Mataga, N.; Asahi, T.; Kanda, Y.; Okada, T.; Kakitani, T. *Chem. Phys.* **1988**, *127*, 249.

0002-7863/93/1515-12137$04.00/0 © 1993 American Chemical Society

top region of the bell-shaped energy-gap dependence predicted by the usual electron-transfer theory. Actually, k_{CR} is comparable with or larger than the corresponding CS rate, k_{CS}.[8-13] Under these circumstances, observation of a transient IP state is often quite difficult even by ultrafast laser photolysis. On the other hand, in less polar solvents like benzene, the CR of the IP state becomes considerably slower, due to the increase of $-\Delta G_{IP}$ and the decrease of the solvent reorganization energy.[8-14] Nevertheless, k_{CR} values in the IP state of various P–Q systems are still much larger than those of typical exciplex systems[15] owing to their relatively small $-\Delta G_{IP}$ values. It is obvious that large k_{CR} values in the IP state, $(P)^+-(Q)^-$, are quite unfavorable for attaining high yields of CS triggered by photoinduced ET in P–Q systems. Accordingly, in order to overcome this cumbersome situation, multistep ET strategies have been used to increase the quantum yield and the lifetime of the final IP state. So far, two types of two-step ET reaction modes are known, as depicted simply by the following eqs 1 and 2,

type a

$$^1(P)^*-Q_1-Q_2 \rightarrow (P)^+-(Q_1)^--Q_2 \rightarrow (P)^+-Q_1-(Q_2)^- \quad (1)$$

type b

$$D-^1(P)^*-Q \rightarrow D-(P)^+-(Q)^- \rightarrow (D)^+-P-(Q)^- \quad (2)$$

where D represents an electron donor to $(P)^+$. In a type a reaction mode, CS between $^1(P)^*$ and Q_1 is followed by a charge shift (CSH) reaction, leading to the formation of the secondary IP state $(P)^+-Q_1-(Q_2)^-$, where $(P)^+$ remains as the positively charged species and CR to the ground state is slower than in the initial IP state because the negatively charged site is shifted farther from $(P)^+$. In a type b mode, hole transfer from $(P)^+$ to D in the initial IP state moves the cation site farther from $(Q)^-$, and P is restored to the ground state, thus leading to an increase in the lifetime of the secondary IP state. In view of the formation of a stable ion pair state (special pair)$^+-(Q_A)^-$ from the first excited singlet state of the special pair via (special pair)$^+$–(bacteriopheophytin)$^-$ in bacterial RC, photosynthetic systems are using a type a mode in their fast CS events.[20]

The first study of a type a ET in artificial systems was made by employing the compound, $P-(CH_2)_4-Q_1-(CH_2)_4-Q_2$ ($P4Q_1$-$4Q_2$) where P, Q_1, and Q_2 represent etioporphyrin, benzoquinone, and trichlorobenzoquinone, respectively.[16] Picosecond laser photolysis studies on this system clearly indicated that the lifetime of the final IP state $(P)^+4Q_14(Q_2)^-$ was longer than that of a reference IP state $[(P)^+-(CH_2)_4-(Q_1)^-$ $((P)^+4(Q_1)^-)]$ due to a greater separation between charges,[9,15a,16] but a difference in lifetimes between the two IP states was not very large. These facts suggested that $P4Q_14Q_2$ could take configurations in which the $(P)^+$ and $(Q_2)^-$ moieties were close to each other, probably because of flexible chains linking the chromophores. Furthermore, in this study the lack of a characteristic sharp absorption band of the radical ion $(Q_1)^-$ and/or $(Q_2)^-$ precluded direct observation of two-step ET process by picosecond laser spectroscopy.

On the other hand, rather extensive works have been carried out on models in which a type b ET sequence provides long-lived IP states. Gust and Moore have synthesized several linked carotenoid–porphyrin–quinone (C–P–Q) models in which multistep ET leads to IP states with long lifetimes.[5,17] They also reported carotenoid–porphyrin–diquinone molecules which, upon excitation, produced even longer-lived IP states.[17f,h,i] However, the mechanistic pathways leading to the ultimate IP state are not clear, owing to lack of ultrafast transient absorption data. Formation of a long-lived IP state by type b ET was also reported in an amine–porphyrin–quinone triad system, in which a dimethylaniline unit acted as an electron donor toward $(P)^+$.[18] We have also made similar studies on some triads with pyromellitimide (Im) as an electron acceptor instead of quinones.[11,19] For example, in the case of a diporphyrin (D)–porphyrin (M)–Im triad system, a long-lived IP state $[(D)^+-M-(Im)^-]$ was formed by a reaction sequence analogous to type b.[11,19d] The lifetime of the $(D)^+$–$M-(Im)^-$ state in one of the triads was 2.5 μs in THF and 8.2 μs in DMF.[11,19d] Thus fairly long-lived final IP states have been produced in the D–M–Im system as well as in the other triads systems which undergo the type b ET. Nevertheless, their quantum yields of the final IP state at room temperature are considerably smaller than that in the biological photosynthetic RC and their reaction mode is different from that in the RC.

In the present work, we have attempted to prepare a new series of photosynthetic triad models in which the final IP state may be formed with a high quantum yield and details of the type a ET dynamics can be observed more clearly by the ultrafast laser spectroscopy than in the case of the $P4Q_14Q_2$ compound. The prepared models, ZnP–Im–Q, where ZnP, Im, and Q represent zinc porphyrin, pyromellitimide, and benzoquinone and its derivatives, respectively, are shown in Chart I. In view of their

(15) (a) Mataga, N. *Pure Appl. Chem.* **1984**, *56*, 1255 and references cited therein. (b) Mataga, N.; Nishikawa, S.; Asahi, T.; Okada, T. *J. Phys. Chem.* **1990**, *94*, 1443. (c) Mataga, N. In *Electron Transfer in Inorganic, Organic and Biological Systems*; Bolton, J. R., Mataga, N., McLendon, G. L., Eds.; Advances in Chemistry Series 228; American Chemical Society: Washington, DC, 1991; Chapter 6, p 91.

(16) Nishitani, S.; Kurata, N.; Sakata, Y.; Misumi, S.; Karen, A.; Okada, T.; Mataga, N. *J. Am. Chem. Soc.* **1983**, *105*, 7771.

(17) (a) Moore, T. A.; Gust, D.; Mathis, P.; Mialocq, J.-C.; Chachaty, C.; Bensasson, R. V.; Land, E. J.; Doizi, D.; Liddell, P. A.; Lehman, W. R.; Nemeth, G. A.; Moore, A. L. *Nature* **1984**, *307*, 630. (b) Seta, P.; Bienvenue, E.; Moore, A. L.; Mathis, P.; Bensasson, R. V.; Liddell, P.; Pessiki, P. J.; Joy, A.; Moore, T. A.; Gust, D. *Nature* **1985**, *316*, 653. (c) Liddell, P. A.; Barrett, D.; Makings, L. R.; Pessiki, P. J.; Gust, D.; Moore, T. A. *J. Am. Chem. Soc.* **1986**, *108*, 5350. (d) Gust, D.; Moore, T. A.; Makings, L. R.; Liddell, P. A.; Nemeth, G. A.; Moore, A. L. *J. Am. Chem. Soc.* **1986**, *108*, 8023. (e) Gust, D.; Moore, T. A.; Liddell, P. A.; Nemeth, G. A.; Makings, L. R.; Moore, A. L.; Barrett, D.; Pessiki, P. J.; Bensasson, R. V.; Rougée, M.; Chachaty, C.; De Schryver, F. C.; Van der Auweraer, M.; Holzwarth, A. R.; Connolly, J. S. *J. Am. Chem. Soc.* **1987**, *109*, 846. (f) Gust, D.; Moore, T. A.; Moore, A. L.; Barrett, D.; Harding, L. O.; Makings, L. R.; Liddell, P. A.; DeSchryver, F. C.; Van der Auweraer, M.; Bensasson, R.; Rougée, M. *J. Am. Chem. Soc.* **1988**, *110*, 321. (g) Gust, D.; Moore, T. A.; Moore, A. L.; Makings, L. R.; Seely, G. R.; Ma, X.; Trier, T. T.; Gao, F. *J. Am. Chem. Soc.* **1988**, *110*, 7567. (h) Gust, D.; Moore, T. A.; Moore, A. L.; Seely, G.; Liddell, P.; Barrett, D.; Harding, L. O.; Ma, X. C.; Lee, S.-J.; Gao, F. *Tetrahedron* **1989**, *45*, 4867. (i) Gust, D.; Moore, T. A.; Moore, A. L.; Lee, S.-J.; Bittersmann, E.; Luttrull, D. K.; Rehms, A. A.; DeGraziano, J. M.; Ma, X. C.; Gao, F.; Belford, R. E.; Trier, T. T. *Science* **1990**, *248*, 199. (j) Hasharoni, K.; Levanon, H.; Tang, J.; Bowman, M. K.; Norris, J. R.; Gust, D.; Moore, T. A.; Moore, A. L. *J. Am. Chem. Soc.* **1990**, *112*, 6477.

(18) (a) Wasielewski, M. R.; Niemczyk, M. P.; Svec, W. A.; Pewitt, E. B. *J. Am. Chem. Soc.* **1985**, *107*, 5562. (b) Wasielewski, M. R.; Gaines, G. L., III; O'Neil, M. P.; Svec, W. A.; Niemczyk, M. P. *J. Am. Chem. Soc.* **1990**, *112*, 4559.

(19) (a) Osuka, A.; Maruyama, K.; Mataga, N.; Asahi, T.; Yamazaki, I.; Nishimura, Y. *Chem. Phys. Lett.* **1991**, *181*, 413. (b) Osuka, A.; Yamada, H.; Maruyama, K.; Mataga, N.; Asahi, T.; Yamazaki, I.; Nishimura, Y. *Chem. Phys. Lett.* **1991**, *181*, 419. (c) Osuka, A.; Nagata, T.; Maruyama, K.; Mataga, N.; Asahi, T.; Yamazaki, I.; Nishimura, Y. *Chem. Phys. Lett.* **1991**, *185*, 88. (d) Osuka, A.; Nakajima, S.; Maruyama, K.; Mataga, N.; Asahi, T.; Yamazaki, I.; Nishimura, Y.; Ohno, T.; Nozaki, K. *J. Am. Chem. Soc.* **1993**, *115*, 4577. (e) Osuka, A.; Nagata, T.; Kobayashi, F.; Zhang, R. P.; Maruyama, K.; Mataga, N.; Asahi, T.; Ohno, T.; Nozaki, K. *Chem. Phys. Lett.* **1992**, *199*, 302.

(20) (a) Kirmaier, C.; Holten, D. *Photosynth. Res.* **1987**, *13*, 225 and references cited therein. (b) Martin, J.-L.; Breton, J.; Hoff, A. J.; Migus, A.; Antonetti, A. *Proc. Natl. Acad. Sci. U.S.A.* **1986**, *83*, 957. (c) Kirmaier, C.; Holten, D. *Proc. Natl. Acad. Sci. U.S.A.* **1990**, *87*, 3552. (d) Holtzapfel, W.; Finkele, U.; Kaiser, W.; Oesterhelt, D.; Scheer, H.; Stilz, H. U.; Zinth, W. *Chem. Phys. Lett.* **1989**, *160*, 1.

(21) (a) Mataga, N.; Okada, T.; Masuhara, H.; Nakajima, N.; Sakata, Y.; Misumi, S. *J. Lumin.* **1976**, *12/13*, 159. (b) Okada, T.; Saito, T.; Mataga, N.; Sakata, Y.; Misumi, S. *Bull. Chem. Soc. Jpn.* **1977**, *50*, 331. (c) Mataga, N.; Migita, M.; Nishimura, T. *J. Mol. Struct.* **1978**, *47*, 199. (d) Okada, T.; Migita, M.; Mataga, N.; Sakata, Y.; Misumi, S. *J. Am. Chem. Soc.* **1981**, *103*, 4715. (e) Migita, M.; Okada, T.; Mataga, N.; Sakata, Y.; Misumi, S.; Nakashima, N.; Yoshihara, K. *Bull. Chem. Soc. Jpn.* **1981**, *54*, 3304.

(22) (a) Verhoeven, J. W. *Pure Appl. Chem.* **1990**, *62*, 1585. (b) Wegewijs, B.; Hermant, R. M.; Verhoeven, J. W.; de Haas, M. P.; Warman, J. M. *Chem. Phys. Lett.* **1990**, *168*, 185. (c) Brouwer, A. M.; Mout, R. D.; Maassen, van den Brink, P. H.; van Ramesdonk, H. J.; Verhoeven, J. W.; Jonker, S. A.; Warman, J. W. *Chem. Phys. Lett.* **1991**, *186*, 481.

(23) Osuka, A.; Marumo, S.; Maruyama, K.; Mataga, N.; Tanaka, Y.; Okada, T., unpublished results.

(24) Masuhara, H.; Ikeda, N.; Miyasaka, H.; Mataga, N. *J. Spectrosc. Soc. Jpn.* **1982**, *31*, 19. (b) Miyasaka, H.; Masuhara, H.; Mataga, N. *Laser Chem.* **1983**, *1*, 357.

Chart I. Structures of Triads Studied in This Work

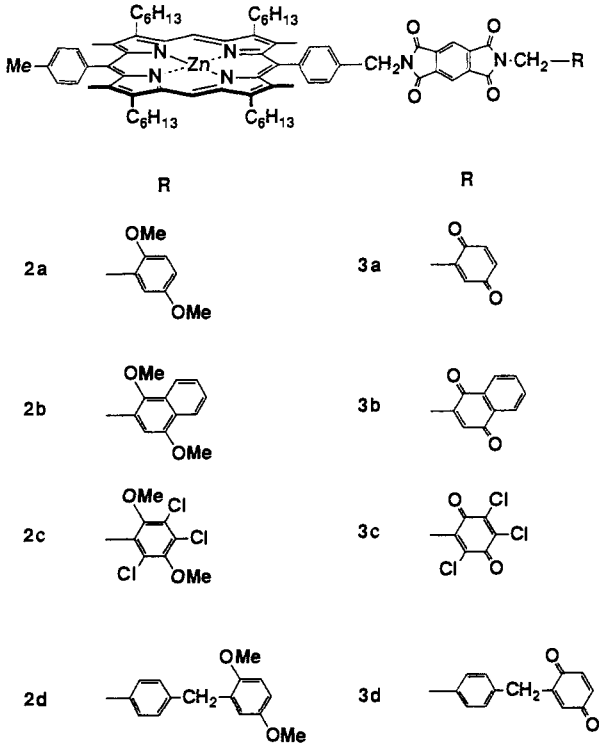

favorable energetics, these triads are expected to undergo a consecutive two-step ET (type a), leading to the formation of the final IP state with a high quantum yield. In addition, the lifetime of $(ZnP)^+$-Im-$(Q)^-$, if actually formed, should be longer than that of a quinone-free reference IP state $(ZnP)^+$-$(Im)^-$. We also expect that the magnitude of the lifetime enhancement in $(ZnP)^+$–Im–$(Q)^-$ compared to $(ZnP)^+$–$(Im)^-$ is greater than that for $(P)^+4Q_1 4(Q_2)^-$ compared to $(P)^+4(Q_1)^-$. This is because, in the former triads, the conformational flexibility is less and therefore the mutual approach between the two ends is less feasible. Both expectations are actually confirmed through this study. Another, more important point in the present investigation is that we have actually succeeded in the direct, unambiguous observation of the type a two-step ET. By using a sharp, characteristic absorption band of $(Im)^-$ appearing at 715 nm,[11,19] we can follow very clearly a two-step ET (CS and subsequent CSH):

$$^1(ZnP)^*\text{–Im–Q} \rightarrow (ZnP)^+\text{–}(Im)^-\text{–Q(IP1)} \rightarrow (ZnP)^+\text{–Im–}(Q)^-\text{(IP2)}$$

It is interesting to note that during the second-step CSH reaction the absorbance of $(ZnP)^+$ retained its intensity essentially unchanged. Such a clear-cut observation would be rather difficult in models containing only quinones as electron acceptors.

2. Results and Discussion

Synthesis of Models. We have studied in this work the porphyrin models **3a–d** shown in Chart I. The synthetic route to **3a** is rather straightforward, as shown in Scheme I. Acid-catalyzed condensation of *p*-tolualdehyde, bis(3-hexyl-4-methyl-2-pyrrolyl)methane, and an aromatic aldehyde (**1a**) in a ratio of 9:10:1, followed by oxidation with *p*-chloranil, gave the porphyrin **2a** in 18% yield.[26] Demethylation with BBr_3 followed by oxidation and zinc metalation in the usual manner furnished porphyrin **3a** in 65% yield. Porphyrins **3b–d** were prepared in a similar manner, and the respective isolated yields are summarized in the Experimental Section. An important feature of the triads studied here is that they are energetically well-defined and their conformations are relatively constrained. Structurally, the meso-aryl substituent is held at nearly perpendicular geometry to the porphyrin plane due to severe steric hindrance between the flanking methyl groups and the aryl bridge, and the center-to-center distances between ZnP and Im and between Im and Q are fixed. It should, however, be noted here that the two CH_2 spacers in **3a–c** allow some conformational freedom, which gives rise to a distribution of ZnP–Q interchromophore distances. In **3a–c**, the Im moiety is linked via a methylene group to the meso-phenyl group as well as to the Q-moiety. On the other hand, the Q-moiety in **3d** is attached to Im across an additional 1,4-phenylene spacer, which provides a greater separation between Im and Q.

Scheme I. Synthesis of Triad **3a**[a]

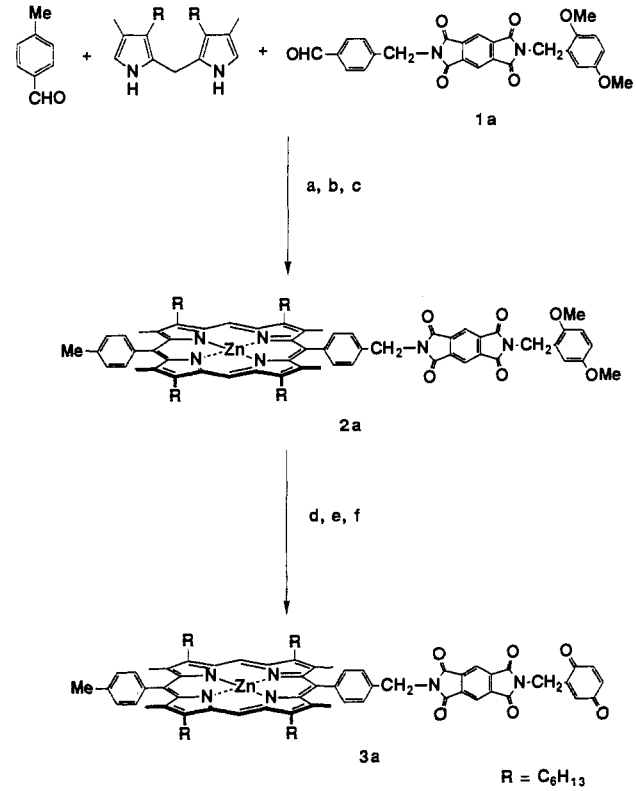

[a] (a) CCl_3CO_2H, CH_3CN, room temperature 16 h; (b) *p*-chloranil, THF, room temperature, 3 h; (c) $Zn(OAc)_2$, MeOH; (d) BBr_3, CH_2Cl_2, –78 °C to room temperature; (e) PbO_2, CH_2Cl_2, room temperature, 2 h; (f) $Zn(OAc)_2$, MeOH.

Energetics in THF Solutions. Free energy gaps for CR of the IP state, $-\Delta G_{IP}$, were evaluated in the usual way[13,14] by using one-electron oxidation and reduction potentials of the relevant chromophores (see footnote *a* in Table I). The Born equation was used for correction of solvation energies, and Coulombic energies were evaluated on the basis of the center-to-center distance between charges estimated from Corey–Pauling–Koltum models. From the excitation energy of the S_1 state of the ZnP chromophore (2.13 eV) and the free energy gap, $-\Delta G_{IP1}$ for CR in IP1 (1.64 eV), that for the CS reaction, $^1(ZnP)^*$–Im–Q → IP1, was calculated to be $-\Delta G_{CS} = 0.49$ eV. The free energy gap, $-\Delta G_{IP2}$, for CR in IP2 and that, $-\Delta G_{CSH}$, for the CSH reaction, IP1 → IP2, are given in Table I. In the estimation of $-\Delta G_{IP2}$, an average value of the center-to-center distance between ZnP and Q (16.0 Å) was used (Table I). If we were to assume the ZnP–Q distance to be 19.2 Å (corresponding to the most extended conformation), then $-\Delta G_{IP2}$ would increase by about 0.02 eV. A key feature in triads **3** is that an energy gradient exists from $^1(ZnP)^*$–Im–Q via $(ZnP)^+$–$(Im)^-$–Q to $(ZnP)^+$–Im–$(Q)^-$: the first free energy gap is constant (0.49 eV), while the second varies from 0.07 eV in **3b** to 0.68 eV in **3c**.

(25) Nagata, T. *Bull. Chem. Soc. Jpn.* **1991**, *64*, 3005.
(26) Osuka, A.; Nagata, T.; Kobayashi, F.; Maruyama, K. *J. Heterocycl. Chem.* **1990**, *27*, 1657.

Table I. Free Energy Gaps for the CR of IP2 State ($-\Delta G_{IP2}$) and for the CSH Reaction from IP1 to IP2 ($-\Delta G_{CSH}$) as well as k_{CSH}, ϕ_2, and ϕ in THF solution

compd	$-\Delta G_{IP2}$ (eV)[a]	$-\Delta G_{CSH}$ (eV)	k_{CSH} (s^{-1})	ϕ_2[b]	ϕ[c]
3a	1.40	0.24	3.0×10^{10}	0.75	0.72
3b	1.57	0.07	2.5×10^{9}	0.20	0.19
3c	0.96	0.68	$>2 \times 10^{11}$	~1	0.96

[a] Values of $-\Delta G_{IP2}$ have been calculated with use of the equations $-\Delta G_{IP2} = E_{ox} - E_{red} + \Delta G_s$, $\Delta G_s = (e^2/2)(1/r_D + 1/r_A)(1/\epsilon - 1/\epsilon_r) - e^2/\epsilon r$, where E_{ox} and E_{red} are respectively the oxidation potential of the ZnP group and reduction potential of each quuinone group measured in DMF, r is the center-to-center distance between the ZnP and quinone chromophores, r_D and r_A are the effective radii of the ZnP cation and quinone anion taken to be 5 and 4 Å, respectively, and ϵ_r and ϵ are the respective dielectric constants of DMF and THF. [b] Quantum yield for the formation of $(ZnP)^+$–Im–$(Q)^-$ from $(ZnP)^+$–$(Im)^-$–Q. [c] Quantum yield for the formation of $(ZnP)^+$–Im–$(Q)^-$ from $^1(ZnP)^*$–Im–Q.

Scheme II. Reaction Scheme for Compounds **3**

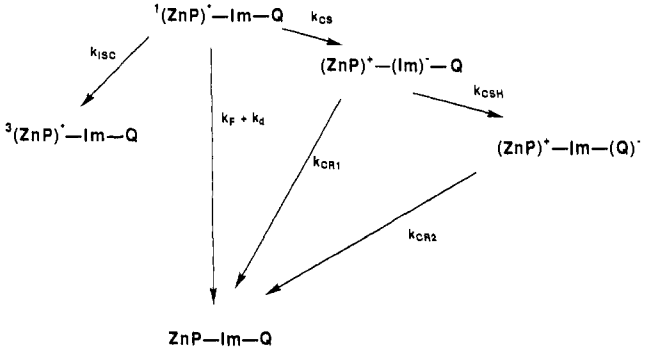

Electron-Transfer Dynamics in THF Solutions. Absorption of light by triads **3** leads to the series of events depicted in Scheme II. Excitation of the zinc porphyrin moiety leads to its first excited singlet state $^1(ZnP)^*$-Im-Q (S_1). Charge separation between $^1(ZnP)^*$ and Im produces, in competition with the deactivation to the ground state as well as intersystem crossing to $^3(ZnP)^*$, the initial IP state $(ZnP)^+$–$(Im)^-$–Q (IP1), whose decay is partitioned between a return to the ground state via CR deactivation (CR1) and formation of the secondary IP state $(ZnP)^+$–Im–$(Q)^-$ (IP2) by the charge shift (CSH) reaction. The IP2 state decays to the ground state via CR2. The lifetimes of the S_1, IP1, and IP2 states are given by τ_{S_1} $[=(k_{CS} + \tau_0^{-1})^{-1}]$, τ_{IP1} $[=(k_{CR1} + k_{CSH})^{-1}]$, and τ_{IP2} $[=k_{CR2}^{-1}]$, respectively, where $\tau_0 = (k_F + k_d + k_{ISC})^{-1}$. The quantum yield for formation of IP1 from S_1 and that for formation of IP2 from IP1 are given by $\phi_1 = \tau_{S1} k_{CS}$ and $\phi_2 = \tau_{IP1} k_{CSH}$, respectively. Thus the net quantum yield for formation of IP2 from S_1 is given by $\phi = \phi_1\phi_2$.

Figure 1 shows the picosecond time-resolved transient absorption spectra for **3d** in THF solution. The 13-ps spectrum shows bleaching of the Q-bands of ZnP at 546 and 583 nm and a distinct transient absorption band centered at 460 nm, both of which appear instantaneously within the excitation flash. This spectrum, which is due to the $S_n \leftarrow S_1$ absorption of ZnP,[19] shows a single exponential decay with $\tau = 60$ ps. As this absorption band decays, a sharp absorption band with a peak at 715 nm due to $(Im)^-$ appears with a risetime of 60 ps. The spectrum in the 600–700-nm region contains substantial absorbance due to $(ZnP)^+$ centered at 677 nm. This absorbance due to the chromophore ion shows single exponential decay with $\tau = 100$ ps (i.e., $k_{CR1} = 1.0 \times 10^{10}\ s^{-1}$). All of these time-dependent spectral changes are virtually identical with those of a quinone-free reference dyad (ZnP–Im) in THF solution,[11] indicating clearly that $k_{CSH} \ll k_{CR1}$ in **3d**. Thus the reaction scheme for **3d** is indistinguishable from that of the reference ZnP–Im system without the CSH and CR2 reactions. We therefore determined the rate constants for the ET reaction occurring in **3d** as follows: $k_{CS} = 1.6 \times 10^{10}\ s^{-1}$ and $k_{CR1} = 1.0 \times 10^{10}\ s^{-1}$ on the basis of the decay rates of the

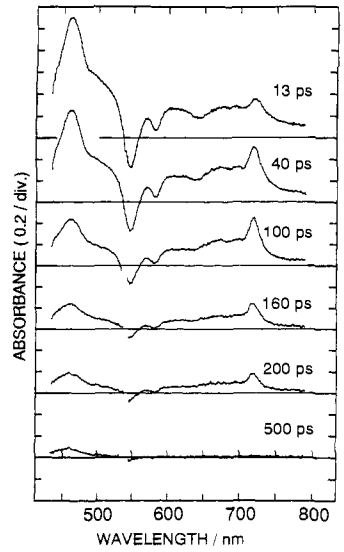

Figure 1. Picosecond time-resolved transient absorption spectra of **3d** in THF solution. The delay times from the exciting pulse are indicated.

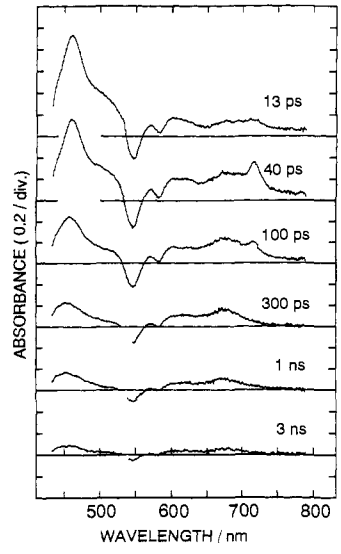

Figure 2. Picosecond time-resolved transient absorption spectra of **3a** in THF solution. The delay times from the exciting pulse are indicated.

S_1 and IP1 states, and $\tau_0 = 1.3$ ns determined by measurement on a reference compound without electron acceptor.

Figure 2 shows the picosecond time-resolved transient absorption spectra for **3a** in THF. The absorption band of **3a** around 460 nm has the same shape and peak position as that of **3d** and can be ascribed mainly to the S_1 state of the ZnP chromophore. As in the case of **3d**, the sharp absorption band of $(Im)^-$ of the IP1 arises at 715 nm, corresponding to the decay of the 460-nm band. However, the $(Im)^-$ band decays much faster than that in **3d**, and a fairly long-lived broad absorption band due to $(ZnP)^+$ around 670 nm was observed after almost complete disappearance of the $(Im)^-$ band. This result indicates that, contrary to the case of **3d**, the IP1 → IP2 CSH process actually occurs in **3a** (Scheme II). The difference in the decay behaviors of IP1 between **3a** and **3d** is ascribed to an extremely slow CSH reaction in the latter, owing to the longer distance between the Im and Q moieties.

According to Scheme II; the time-dependent concentrations of the S_1, IP_1, and IP_2 states are given by the following eqs 3–5:

$$[S_1(t)] = A_0 \exp(-t/\tau_{S_1}), \quad A_0 = [S_1(0)] \tag{3}$$

$$[IP1(t)] = \frac{A_0\phi_1\tau_{S_1}^{-1}}{(\tau_{S_1}^{-1} - \tau_{IP1}^{-1})}[\exp(-t/\tau_{IP1}) - \exp(-t/\tau_{S1})] \tag{4}$$

$$[\mathrm{IP2}(t)] = \frac{A_0\phi_1\phi_2\tau_{S_1}^{-1}\tau_{IP1}^{-1}}{(\tau_{S1}^{-1} - \tau_{IP1}^{-1})}\left[\frac{\exp(-t/\tau_{S1}) - \exp(-t/\tau_{IP2})}{(\tau_{S_1}^{-1} - \tau_{IP2}^{-1})} - \frac{\exp(-t/\tau_{IP1}) - \exp(-t/\tau_{IP2})}{(\tau_{IP1}^{-1} - \tau_{IP2}^{-1})}\right] \quad (5)$$

The time profile of the transient absorbance at a wavelength is given by using the respective difference absorption coefficients of the S_1 state (ϵ_{S_1}) and the IP states (ϵ_{IP1} and ϵ_{IP2}) at that wavelength as follows:

$$A(t) = \epsilon_{S1}[S_1(t)] + \epsilon_{IP1}[\mathrm{IP1}(t)] + \epsilon_{IP2}[\mathrm{IP2}(t)] \quad (6)$$

With these equations, it is evident that $A(t)$ can be expressed by a linear combination of three exponentials with time constants of τ_{S_1}, τ_{IP1} and τ_{IP2}. ϵ_{S_1} was determined by measurements of the transient absorbance and ground-state bleaching as well as their excitation-intensity dependence of the ZnP reference compounds in THF for S_1, ϵ_{IP} due to $(ZnP)^+$ was determined by a similar measurement on the IP2 state in **3a** in THF, and ϵ_{IP} due to $(Im)^-$ was determined by the transient absorbance measurement on $(Im)^-$ produced by intermolecular ET quenching of excited *N,N'*-dihexylpyromellitimide (a reference Im molecule) with N,N-dimethylaniline in THF solution.

We have analyzed the time profiles of the transient absorbances of **3a** on the basis of the above equations. In the first place, the decay profile of the 460-nm band of **3a** is very similar to that of **3d**, indicating that the CS and CR1 processes in **3a** are practically the same as those in **3d**. From the initial decay time of $\tau_{S_1} = 55$ ps at 460 nm observed for **3a** and $\tau_0 = 1.3$ ns, k_{CS} has been determined to be 1.7×10^{10} s^{-1}. With respect to k_{CR1}, we take the same rate as in **3d**, viz., 1.0×10^{10} s^{-1}. For the determination of τ_{IP1}, we have examined the time profile of the $(Im)^-$ absorbance at 715 nm on the basis of eq 4, taking into consideration the time response of the apparatus. By this analysis, we have obtained the rise and decay times of the absorbance at 715 nm to be 25 and 55 ps, respectively. The decay time agrees with the decay time of the S_1 state, τ_{S_1}. According to eq 4, this means that $\tau_{IP1} < \tau_{S1}$ and, therefore, $\tau_{IP1} = 25$ ps. With this τ_{IP1} value and the value of $k_{CR1} = 1.0 \times 10^{10}$ s^{-1}, we have evaluated k_{CSH} in **3a** to be 3.0×10^{10} s^{-1}. By using these ET rate constants in **3a**, we have obtained the quantum yields of IP formation in **3a** as follows: $\phi_1 = 0.96$, $\phi_2 = 0.75$, and $\phi = \phi_1\phi_2 = 0.72$.

We have also examined the decay process of the IP2 state by measuring the time profile of a broad band due to $(ZnP)^+$ centered at 677 nm. We have observed a double exponential decay with time constants of 600 ps and 4 ns with component fractions of 0.53 and 0.47, respectively. We infer that these kinetics reflect the existence of different conformers in IP2, which probably give rise to two (average) k_{CR2} values, originating from a distribution of center-to-center distances between ZnP and Q.

Thus, the conformation distribution seems possible to some extent owing to internal rotation around the two–CH_2– groups, although the conformational flexibility of the present triads may be less than that in $P4Q_14Q_2$, as described in the Introduction. The observed long-lived and short-lived components in the decay of the IP2 state might be ascribed to extended and shrunk conformers, respectively. In the typical intramolecular exciplex systems,[15,21] D–$(CH_2)_n$–A, where A is aromatic hydrocarbon and D is *N,N*-dimethylaniline groups, as well as some related compounds,[22] the dynamic process of conformational changes from extended to shrunk forms affects significantly the CR of the IP state. In some intramolecular exciplex systems in polar solutions, the CR rate is enhanced by such conformational changes.[15,21] However, even in the simple D–$(CH_2)_n$–A system (with $n = 2,3$) in nonviscous polar solutions, it takes more than a few nanoseconds for the conformational changes.[15,21] Therefore, the dynamic processes of the conformational changes may not be important for shortening the lifetime of the IP2 state to between several hundred picoseconds and several nanoseconds, but the different conformers may be present already in the ground state.

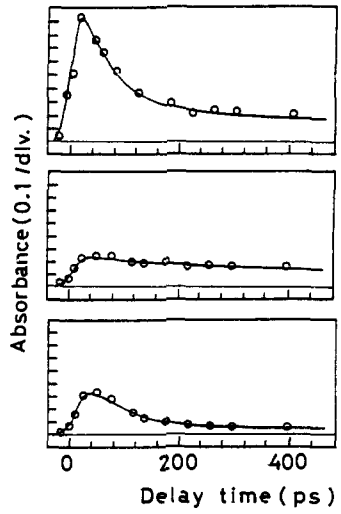

Figure 3. Time profiles of transient absorbance (O) of **3a** in THF solution at 460, 677, and 715 nm (from top to bottom frame) and their simulation (—) (see text).

At this point, one may argue that studies on temperature dependencies of ET processes in the present system may be very useful in comparing their character with bacterial photosynthetic RC and also in examining the effect of the conformational changes from extended to shrunk forms in the IP2 state.

However, such measurements in polar solvent, THF, should be quite complicated by the relatively large influence of the temperature dependence of the solvent dielectric properties, which will affect the energy gaps and solvent reorganization energy, etc., making it difficult to derive a reliable conclusion from these observations. Even if one could obtain some results, they would be very similar to those of our previous studies on porphyrin–quinone dyads:[13] decrease of the activation energy with increase of the energy gap for CSH reaction in the normal region (see also Table I and Concluding Remarks), very small activation energy in the case of **3c**, and activationless reaction for the CR of the IP in the inverted region.

The studies of the temperature effects will also not be useful for the problem of the conformational changes in the IP2 state owing to the same complications caused by the temperature dependence of the solvent dielectric properties. As stated above, we can conclude that the conformational changes in the IP2 state of the present systems will be much slower than the fast CR and also slower than the slow CR on the basis of the previous studies of the much simpler intramolecular exciplex systems.[21,22]

By using the values of rate constants and/or lifetimes of the transient states as well as the values of extinction coefficients of those transient states obtained above for **3a**, we can simulate observed time profiles of the absorbance changes at various wavelengths. Specifically, the observed time profiles at 460, 677, and 715 nm and their simulated curves evaluated by taking into account the response time of the apparatus are shown in Figure 3. Our analysis of all the kinetic results for **3a** seems to be consistent as a whole.

The picosecond time-resolved absorption spectra of **3c** in THF solution are displayed in Figure 4. The time profile and band shape of the absorption at 460 nm are very similar to those of **3a**, and the time constants of initial decay within the ZnP–Im pair in **3c** can be deemed to be the same as those in **3a**. Importantly, however, we cannot recognize the rise of the $(Im)^-$ band, but we can see the rise of the 677-nm band due to $(ZnP)^+$, the kinetics of which corresponds to the decay of the 460-nm band. This result means that the CSH reaction from IP1 to IP2 in **3c** is much

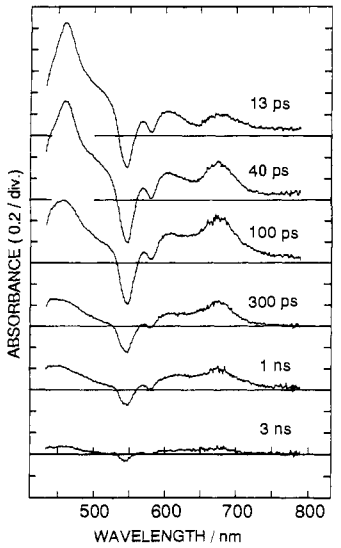

y = 205q

Figure 4. Picosecond time-resolved transient absorption spectra of **3c** in THF solution. The delay times from the exciting pulse are indicated.

faster than the CS reaction from S_1 to IP1, owing to a much larger energy gap for the former.

In an analogous fashion to the analysis of **3a**, we take $k_{CS} = 1.7 \times 10^{10}$ s^{-1} and $k_{CR1} = 1.0 \times 10^{10}$ s^{-1} also in **3c**, and we have attempted to analyze the time profiles of the transient absorbance at 460, 677, and 715 nm in **3c** on the basis of eq 6. The simulation of the rise and decay of the transient absorbance at 715 nm indicated a risetime shorter than 5 ps and a decay time of 55 ps. This result means that $k_{CSH} > 2 \times 10^{11}$ s^{-1} and $\phi_2 \approx 1$, leading to $\phi = \phi_1\phi_2 \approx 0.96$ in **3c**. The results of simulation of $A(t)$ at 460 and 677 nm have indicated a double exponential decay of IP2 similar to the case of **3a** with time constants of 900 ps and 4 ns with components fractions of 0.57 and 0.43, respectively.

In essentially the same manner, the ET dynamics of **3b** have also been analyzed, and the results obtained are summarized in Table I (the transient absorption spectra, which are quite similar to those of **3a**, are not shown). The quantum yield ϕ_2 is low, presumably due to an insufficient energy gap for CSH, the rate of which we have estimated is 2.5×10^9 s^{-1}.

Concluding Remarks. Electron-transfer processes such as photoinduced CS, CR, and CSH in the various IP states are regulated by a variety of parameters. These include the free energy gap, $-\Delta G$, between the initial and final states of the electron transfer; the magnitudes of electronic interactions between the chromophores involved, which are dependent on the mutual distance and orientation; the reorganization energies; the temperature; and also the solvent dynamics. By controlling these factors in a molecular design to simulate the multichromophoric arrays in biological RC models, it is possible for biomimetic CS in artificial models to approach ultrafast and virtually quantitative production of a stabilized IP state. In the present work, we have demonstrated unambiguously for the first time formation of a fairly long-lived IP state by a two-step ET reaction of the type essentially similar to that occurring in biological RC by employing the ZnP–Im–Q triads. This was possible only because the very characteristic, sharp absorption of $(Im)^-$ functioned as a direct indicator of ET processes. The lifetime enhancement in $(ZnP)^+$–Im–$(Q)^-$ compared to $(ZnP)^+$–$(Im)^-$ (from 100 to 4000 ps of the long-lived species) is considerably larger than that for $(P)^+4Q_14(Q_2)^-$ compared to $(P)^+$–$4(Q_1)^-$ (from ~100 to 400 ps)[9,15a] due to the lower conformational flexibility in the former triads. Nevertheless, the lifetimes of the IP2 state in the present triads are much shorter than those in some other triads, e.g., $(D)^+$–M–$(Im)^-$.[11,19d] This may be ascribed to the lower rigidity and much shorter distance between the positive and negative charge centers in IP2 (16 Å in IP2 and ~30 Å in the latter triad). Therefore, formation of a more long-lived IP state by type a ET processes may be possible by using a more rigid multichromophoric system with longer distances between the charged centers. On the other hand, we have demonstrated very clearly that the quantum yield for formation of IP2 can be controlled by adjusting the reduction potential of the acceptor, and we have actually realized a virtually quantitative quantum yield for the formation of the secondary IP state in **3c**. With respect to the CSH reaction, inspection of Table I shows that, in these triads, the rate constant increases with the energy gap. Although too few data points are available to obtain the rate constants vs energy gap relation, it is clear that, up to an energy gap of 0.68 eV, there is no evidence for inverted behavior.

On the basis of these present results as well as earlier ones, we are nearing realization of ultrafast and highly efficient formation of long-lived IP states in multichromophoric systems. Actually, we have observed very recently type a ET processes in other triad model compounds,[23] in which the initial CS occurs between chlorophyll-like chromophores and then the CS state thus formed is stabilized by CSH to an attached acceptor, in a manner more closely mimicking the biological RC. Further works directed toward achieving these goals are currently in progress.

3. Experimental Section

UV–visible spectra were recorded with a Shimadzu UV-3000 spectrometer, and the steady-state fluorescence spectra were taken on a Shimadzu RF-502A spectrofluorimeter. ^{1}H-NMR spectra were recorded on a JEOL GX-400 spectrometer (operating at 400 MHz), chemical shifts being reported on the δ scale in ppm relative to internal Me_4Si. Mass spectra were recorded on a JEOL HX-110 spectrometer. For the porphyrin compounds, the positive FAB (fast atom bombardment) ionization method was used, with an accelerating voltage of 10 kV and Xe atoms as the primary ion source. The FAB matrix was 3-nitrobenzyl alcohol/chloroform.

Acetonitrile for synthetic use was refluxed and distilled from P_2O_5. Other solvents and chemicals were reagent grade. Preparative separations were usually performed by using flash column chromatography on silica gel (Merck, kieselgel 60H, Art. 7736).

Picosecond transient absorption spectra were measured on ca. 10^{-4} nitrogen-bubbled solutions by means of a microcomputer-controlled, double-beam picosecond spectrometer with a repetitive, mode-locked Nd^{3+}:YAG laser.[24] The second harmonic of the Nd^{3+}:YAG laser pulse was used for excitation.

Preparation of Porphyrins 2a–d. The synthesis of **2a** is described as a typical procedure. The aromatic aldehyde **1a** (0.1 mmol, 46 mg), bis(3-hexyl-4-methyl-2-pyrrolyl)methane[25] (1 mmol, 342 mg), and *p*-tolualdehyde (0.9 mmol, 98 μL) were dissolved in CH_3Cl–C_6H_6 (15 mL, 36 mL) under nitrogen. To this solution was added trichloroacetic acid (0.1 mmol, 16 mg) in CH_3CN (0.16 mL), and the resulting mixture was stirred for 16 h at room temperature in the dark. *p*-Chloranil (2.0 mmol, 500 mg) was then added, and the resulting mixture was stirred again for 3 h. The solvent was evaporated on a rotary evaporator, and the resulting residue was roughly purified on an alumina short column with CH_2Cl_2 as an eluent. After metalation with $Zn(OAc)_2$, zinc porphyrin products were separated by flash column chromatography (silica gel, CH_2Cl_2). Recrystallization from CH_2Cl_2–*n*-hexane gave **2a** (24 mg, 18% yield based on the amount of **1a** used): mp 130–132 °C; mass *m/z* 1308 (M^+) (calcd for $C_{81}H_{95}N_6O_6Zn$ = 1308.6); ^{1}H-NMR ($CDCl_3$) 10.12 (s, 2H, meso), 8.03 (m, 4H, Ar), 7.70 (d, 2H, J = 8.1 Hz, Ar), 7.55 (d, 2H, J = 7.7 Hz, Ar), 6.74 (m, 2H, Ar), 6.66 (d, 1H, J = 2.6 Hz, Ar), 5.15 (s, 2H, CH_2), 4.76 (s, 2H, CH_2), 3.92 (m, 8H, CH_2), 3.78 (s, 3H, CH_3), 3.70 (s, 3H, CH_3), 2.74 (s, 3H, CH_3) 2.48 (s, 6H, CH_3), 2.37 (s, 6H, CH_3), 2.16 (m, 8H, CH_2), 1.74 (m, 8H, CH_2), 1.47 (m, 8H, CH_2), 1.38 (m, 8H, CH_2), and 0.91 (m, 12H, CH_3).

For **2b–d**, only the physical properties are reported here. **2b** (yield 22%): mp 150–151 °C; mass *m/z* 1358 (M^+) (calcd for $C_{85}H_{99}N_6O_6Zn$ = 1358.6); ^{1}H-NMR ($CDCl_3$) 10.12 (s, 2H, meso), 8.17 (d, 1H, J = 7.6 Hz, Ar), 8.07, (s, 2H, Ar), 8.04 (d, 2H, J = 7.9 Hz, Ar), 7.97 (d, 1H, Ar), 7.94 (d, 2H, J = 7.9 Hz, Ar), 7.70 (d, 2H, J = 7.9 Hz, Ar), 7.54 (d, 2H, J = 7.6 Hz, Ar), 7.50 (dd, 1H, J = 1.2, 8.2 Hz, Ar), 7.47 (dd, 1H, J = 1.2, 8.2 Hz, Ar), 6.63 (s, 1H, Ar), 5.18 (s, 2H, CH_2), 4.89 (s, 2H, CH_2), 3.95 (s, 3H, CH_3), 3.91 (m, 8H, CH_2), 3.89 (s, 3H, CH_3), 2.73 (s, 3H, CH_3) 2.47 (s, 6H, CH_3), 2.36 (s, 6H, CH_3), 2.15 (m, 8H,

CH_2), 1.73 (m, 8H, CH_2), 1.49 (m, 8H, CH_2), 1.38 (m, 8H, CH_2), and 0.91 (m, 12H, CH_3).

2c (yield 22%): mp 143–145 °C; mass *m/z* 1410 (M^+) (calcd for $C_{82}H_{95}N_6O_6Cl_3Zn$ = 1410.5); ^{1}H-NMR ($CDCl_3$) 10.14 (s, 2H, meso), 8.15 (s, 2H, Ar), 8.05 (d, 2H, *J* = 7.7 Hz, Ar), 7.93 (d, 2H, *J* = 7.7 Hz, Ar), 7.01 (d, 2H, *J* = 8.1 Hz, Ar), 7.54 (d, 2H, *J* = 7.7 Hz, Ar), 5.20 (s, 2H, CH_2), 4.97 (s, 2H, CH_2), 3.93 (m, 8H, CH_2), 3.89 (s, 3H, CH_3), 3.89 (s, 3H, CH_3), 2.73 (s, 3H, CH_3) 2.47 (s, 6H, CH_3), 2.37 (s, 6H, CH_3), 2.17 (m, 8H, CH_2), 1.73 (m, 8H, CH_2), 1.49 (m, 8H, CH_2), 1.38 (m, 8H, CH_2), and 0.91 (m, 12H, CH_3).

2d (yield 43%): mp 126–127 °C; mass *m/z* 1398 (M^+) (calcd for $C_{88}H_{100}N_6O_6Zn$ = 1398.6); ^{1}H-NMR ($CDCl_3$) 10.09 (s, 2H, meso), 8.02 (d, 2H, *J* = 8.1 Hz, Ar), 7.96 (d, 2H, *J* = 7.7 Hz, Ar), 7.67 (s, 2H, Ar), 7.63 (d, 2H, *J* = 7.7 Hz, Ar), 7.56 (d, 2H, *J* = 7.7 Hz, Ar), 7.18 (d, 2H, *J* = 7.9 Hz, Ar), 7.09 (d, 2H, *J* = 8.1 Hz, Ar), 6.68 (d, 1H, *J* = 9.9 Hz, Ar), 6.62 (s, 1H, Ar), 6.54 (d, 1H, *J* = 2.5 Hz, Ar), 5.02 (s, 2H, CH_2), 4.53 (s, 2H, CH_2), 3.92 (m, 8H, CH_2), 3.82 (s, 2H, CH_2), 3.67 (s, 3H, CH_3), 3.65 (s, 3H, CH_3), 2.75 (s, 3H, CH_3) 2.48 (s, 6H, CH_3), 2.34 (s, 6H, CH_3), 2.17 (m, 8H, CH_2), 1.75 (m, 8H, CH_2), 1.48 (m, 8H, CH_2), 1.40 (m, 8H, CH_2), and 0.93 (m, 12H, CH_3).

Preparation of Porphyrins 3a–d. The synthesis of **3a** is described here as a typical procedure. Porphyrin **2a** (10 μmol, 13 mg) was dissolved in dry CH_2Cl_2 (10 mL), and the solution was cooled to −78 °C under nitrogen. To this solution was added BBr_3 (3.2 mmol, 0.3 mL) in CH_2Cl_2 (10 mL) slowly in the dark. The reaction mixture was stirred for 1 h at the same temperature and was later allowed to warm to room temperature. The reaction mixture was then cooled to 0 °C, and water was added carefully to quench the excess BBr_3. The organic layer was separated, and the aqueous layer was further extracted with CH_2Cl_2 (2 × 15 mL). The organic layers were combined, washed with water and aqueous $NaHCO_3$, dried over anhydrous Na_2SO_4, and taken to dryness on a rotary evaporator. The hydroquinone-linked porphyrin product was quickly purified by flash column chromatography (silica gel, CH_2Cl_2), dissolved in CH_2Cl_2 and oxidized with PbO_2 (4.2 μmol, 10 mg) under nitrogen. The reaction mixture was stirred for 2 h in the dark at room temperature. PbO_2 was filtered off, and the filtrate was treated with $Zn(OAc)_2$. Porphyrin **3a** was purified by flash column chromatography (silica gel, CH_2Cl_2). Recrystallization from CH_2Cl_2–*n*-hexane gave **3a** (6.5 μmol, 9 mg, 65% yield based on the amount of **2a** used). Since the mass peaks of the zinc complexes **3a–d** were too weak for high-resolution FAB mass measurement (HRFABMS), we measured HRFABMS for the corresponding free based compounds. **3a**: mp 144–146 °C; mass *m/z* 1280 (M^+ + 1) (calcd for $C_{79}H_{89}N_6O_6Zn$ = 1280.6); ^{1}H-NMR ($CDCl_3$) 10.16 (s, 2H, meso), 8.40 (s, 2H, Ar), 8.06 (d, 2H, *J* = 8.1 Hz, Ar), 7.93 (d, 2H, *J* = 7.3 Hz, Ar), 7.75 (d, 2H, *J* = 8.6 Hz, Ar), 7.54 (d, 2H, *J* = 8.1 Hz, Ar), 7.93 (d, 2H, *J* = 7.3 Hz, Ar), 7.75 (d, 2H, *J* = 8.6 Hz, Ar), 7.54 (d, 2H, *J* = 8.1 Hz, Ar), 6.84 (m, 2H, Ar), 6.79 (d, 1H, *J* = 2.1 Hz, Ar), 5.29 (s, 2H, CH_2), 4.76 (s, 2H, CH_2), 3.94 (m, 8H, CH_2), 2.73 (s, 3H, CH_3) 2.48 (s, 6H, CH_3), 2.39 (s, 6H, CH_3), 2.15 (m, 8H, CH_2), 1.72 (m, 8H, CH_2), 1.51 (m, 8H, CH_2), 1.39 (m, 8H, CH_2), and 0.90 (m, 12H, CH_3); HRFABMS for the free base complex *m/z* 1219.697 (M^+ + 3) (calcd for $C_{79}H_{91}N_6O_6$ = 1219.700). For **3b–d**, only the physical properties are reported here. **3b** (yield 78%): mp 139–141 °C; mass *m/z* 1330 (M^+ + 2) (calcd for $C_{83}H_{100}N_6O_6Zn$ = 1330.6); ^{1}H-NMR ($CDCl_3$) 10.16 (s, 2H, meso), 8.44 (s, 2H, Ar), 8.14 (m, 1H, Ar), 8.07 (m, 5H, Ar), 7.93 (d, 2H, *J* = 7.7 Hz, Ar), 7.78 (m, 4H, Ar), 7.53 (d, 2H, *J* = 7.7 Hz, Ar), 6.64 (m, 1H, Ar), 6.64 (s, 1H, Ar), 5.30 (s, 2H, CH_2), 4.93 (s, 2H, CH_2), 2.73 (s, 3H, CH_3) 2.47 (s, 6H, CH_3), 2.39 (s, 6H, CH_3), 2.17 (m, 8H, CH_2), 1.73 (m, 8H, CH_2), 1.52 (m, 8H, CH_2), 1.38 (m, 8H, CH_2), and 0.90 (m, 12H, CH_3); HRFABMS for the free base complex *m/z* 1268.709 (M^+ + 2) (calcd for $C_{83}H_{92}N_6O_6$ = 1268.708).

3c (yield 57%): mp 165–167 °C; mass *m/z* 1382 (M^+ + 1) (calcd for $C_{79}H_{85}N_6O_6Cl_3Zn$ = 1382.4); ^{1}H-NMR ($CDCl_3$) 10.16 (s, 2H, meso), 8.34 (s, 2H, Ar), 8.05 (d, 2H, *J* = 8.1 Hz, Ar), 7.93 (d, 2H, *J* = 7.7 Hz, Ar), 7.74 (d, 2H, *J* = 8.1 Hz, Ar), 7.54 (d, 2H, *J* = 8.1 Hz, Ar), 5.27 (s, 2H, CH_2), 4.96 (s, 2H, CH_2), 3.95 (m, 8H, CH_2), 2.73 (s, 3H, CH_3) 2.47 (s, 6H, CH_3), 2.38 (s, 6H, CH_3), 2.14 (m, 8H, CH_2), 1.73 (m, 8H, CH_2), 1.47 (m, 8H, CH_2), 1.38 (m, 8H, CH_2), and 0.90 (m, 12H, CH_3); HRFABMS for the free base complex *m/z* = 1321.578 (M^+ + 3) (calcd for $C_{79}H_{88}N_6O_6Cl_3$ = 1321.583).

3d (yield 65%): mp 120–121 °C; mass *m/z* 1369 (M^+ + 1) (calcd for $C_{86}H_{93}N_6O_6Zn$ = 1369.6); ^{1}H-NMR ($CDCl_3$) 10.14 (s, 2H, meso), 8.21 (s, 2H, Ar), 8.04 (d, 2H, *J* = 7.8 Hz, Ar), 7.93 (d, 2H, *J* = 7.8 Hz, Ar), 7.71 (d, 2H, *J* = 7.8 Hz, Ar), 7.54 (d, 2H, *J* = 7.8 Hz, Ar), 7.37 (d, 2H, *J* = 8.3 Hz, Ar), 7.13 (d, 2H, *J* = 8.3 Hz, Ar), 7.72 (d, 1H, *J* = 10.3 Hz, Ar), 6.65 (dd, 1H, *J* = 7.44, 10.25 Hz, Ar), 6.27 (s, 1H, Ar), 5.21 (s, 2H, CH_2), 4.79 (s, 2H, CH_2), 3.93 (m, 8H, CH_2), 3.68 (s, 2H, CH_2), 2.73 (s, 3H, CH_3) 2.47 (s, 6H, CH_3), 2.37 (s, 6H, CH_3), 2.14 (m, 8H, CH_2), 1.72 (m, 8H, CH_2), 1.47 (m, 8H, CH_2), 1.39 (m, 8H, CH_2), and 0.90 (m, 12H, CH_3); HRFABMS for the free base complex *m/z* = 1308.732 (M^+ + 2) (calcd for $C_{86}H_{96}N_6O_6$ = 1308.739).

Acknowledgment. This work was partly supported by a Grants-in-Aid for Specially promoted Research No. 02102005 and No. 6265006 as well as a Grant-in-Aid for Scientific Research on New Program (03NP0301) from the Ministry of Education, Science and culture of Japan. The authors are grateful to Mr. T. Asahi of Osaka University for his helpful discussions on ET kinetics.